High resolution micro ultrasonic machining for trimming 3D microstructures

2014 J. Micromech. Microeng. 24 065017

(http://iopscience.iop.org/0960-1317/24/6/065017)

IOP Publishing Journal of Micromechanics and Microengineering
J. Micromech. Microeng. **24** (2014) 065017 (8pp) doi:10.1088/0960-1317/24/6/065017

High resolution micro ultrasonic machining for trimming 3D microstructures

Anupam Viswanath, Tao Li and Yogesh Gianchandani

Center for Wireless Integrated MicroSensing and Systems (WIMS^2) and Department of Electrical Engineering and Computer Science, University of Michigan, Ann Arbor, MI, USA

E-mail: anupamv@umich.edu

Received 9 December 2013, revised 20 April 2014
Accepted for publication 23 April 2014
Published 14 May 2014

Abstract
This paper reports on the evaluation of a high resolution micro ultrasonic machining (HR-μUSM) process suitable for post fabrication trimming of complex 3D microstructures made from fused silica. Unlike conventional USM, the HR-μUSM process aims for low machining rates, providing high resolution and high surface quality. The machining rate is reduced by keeping the micro-tool tip at a fixed distance from the workpiece and vibrating it at a small amplitude. The surface roughness is improved by an appropriate selection of abrasive particles. Fluidic modeling is performed to study interaction among the vibrating micro-tool tip, workpiece, and the slurry. Using 304 stainless steel (SS304) tool tips of 50 μm diameter, the machining performance of the HR-μUSM process is characterized on flat fused silica substrates. The depths and surface finish of machined features are evaluated as functions of slurry concentrations, separation between the micro-tool and workpiece, and machining time. Under the selected conditions, the HR-μUSM process achieves machining rates as low as 10 nm s^{-1} averaged over the first minute of machining of a flat virgin sample. This corresponds to a mass removal rate of $\approx$20 ng min^{-1}. The average surface roughness, S_a, achieved is as low as 30 nm. Analytical and numerical modeling are used to explain the typical profile of the machined features as well as machining rates. The process is used to demonstrate trimming of hemispherical 3D shells made of fused silica.

Keywords: ceramic micromachining, ultrasonic-micromachining, high resolution trimming, hemispherical shells

(Some figures may appear in colour only in the online journal)

1. Introduction

Ceramic materials are appealing for use in MEMS because of high chemical inertness, corrosion resistance, oxidation resistance, strength to weight ratio, stiffness, hardness, and the retention of these properties at elevated temperatures [1]. Several types of ceramics have found applications in electronics and MEMS packaging [2–4]. Piezoelectric ceramic materials, such as lead zirconate titanate (PZT), have been widely used in the fabrication of micromachined sensors and actuators [5]. For example, micromachined PZT discs were used as a bulk tissue contrast sensor for fine needle biopsy [6]. Fused silica has several attractive features for use in resonators. It has small linear expansion coefficient ($\alpha_{FS} = 0.5 \times 10^{-6}$ K^{-1}) and thermal conductivity ($k_{FS} =$ 1.38 W m^{-1} K^{-1}). It also has superior thermal shock resistance, allowing quick reflow of the material into a variety of 3D geometries. These properties have allowed the use of molded fused silica in applications such as 3D resonator micro-gyroscopes with quality factors (Q) >100 K [7].

Micro ultrasonic machining (μUSM) has been widely demonstrated as an effective fabrication method for devices made from ceramics such as fused silica. These ceramic materials are mostly transparent, insulating, and brittle and are not well suited for machining by laser, electrodischarge machining, or micromilling/drilling. The μUSM process is appropriate for micromachining both planar and 3D structures of brittle materials without inducing stress or subsurface cracks [8–11]. The machined features can have an average surface roughness as low as 0.25 μm [12]. These factors make μUSM appealing for high resolution and precision machining of ceramics in MEMS.

In conventional USM [13–17], a tool is vibrated along its longitudinal axis, usually at 20 kHz, with an amplitude ranging from 10–50 μm [18, 19]. An abrasive slurry is pumped around the cutting zone. This slurry is comprised of a mixture of abrasive material, e.g. silicon carbide, boron carbide, etc suspended in water or oil. The vibration of the tool imparts kinetic energy to the abrasive particles held in the slurry between the tool and the workpiece, which impact the workpiece surface causing material removal by microchipping [20]. Conventional μUSM typically aims to rapidly remove material, with typical machining rates of >200 nm s^{-1}. The average surface roughness achievable using conventional μUSM is typically 200–400 nm [8–11].

Further refinement of μUSM that leads to high resolution μUSM (HR-μUSM) is of potential interest for a number of MEMS applications. In particular, it is appealing for the post-fabrication trimming of inertial sensors, timing references and mass-balance resonators to adjust stiffness, mass and potentially damping [21, 22]. The two most important attributes of HR-μUSM are low machining rates, and smooth surfaces. Low machining rates can provide improved control of machining in the vertical (depth) direction. While the lateral feature sizes depend on the cutting tools, the material removal rate is determined mainly by the impact velocity of the abrasive particles. This velocity is a function of the frequency and the amplitude of the vibrating tool as well as the separation between the tool and the workpiece [23]. In contrast, the surface finish depends on the particle size of the abrasive used in the ultrasonic machining.

This paper[1] aims at three specific goals. (1) A quantitative evaluation of the impact of particle size, slurry behavior, micro-tool position, and micro-tool amplitude on machining rates and surface roughness. (2) The identification and evaluation of a suitable instrument configuration and interface for HR-μUSM. (3) Evaluation of the ability of HR-μUSM to trim complex 3D fused silica microstructures. In this context, trimming is defined as the procedure by which small quantities of mass can be removed from selected locations. A number of parameters are investigated: (1) tool miniaturization; (2) micro-tool position; (3) vibration amplitude; (4) size of abrasive particles; (5) fluid dynamics of the slurry. The HR-μUSM concept is illustrated in figure 1. The micro-tool tip is positioned at a predefined fixed distance (FD) from the workpiece, without micro-tool feed toward the workpiece as in conventional μUSM. Low vibration amplitudes and small abrasive particles are used to further reduce the machining rates and provide superior surface finish. The design considerations along with analytical and numerical modeling are presented in section 2. The experimental evaluation of the HR-μUSM process is described in section 3. Section 3 also describes the application of HR-μUSM for trimming of hemispherical 3D microstructures. The discussion and conclusions are provided in section 4.

[1] Portions of this paper appear in conference abstract form in [24].

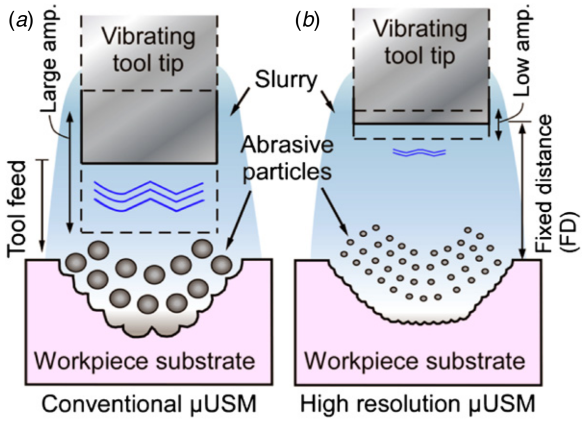

Figure 1. Conceptual comparison of μUSM used for conventional μUSM and for HR-μUSM. (*a*) Conventional μUSM produces deeper machined features with rougher surfaces. (*b*) HR-μUSM uses greater, fixed, distances between tool and workpiece, smaller abrasive particles and lower tool vibration amplitude.

2. Design considerations

2.1. Analytical study

Various analytical models exist in literature to predict the machining rates of stationary μUSM as a function of process parameters. A majority of these are first order models based on statistical analysis and provide an estimation of USM behavior. Shaw's model provides an equation for material removal rate due to hammering action of the abrasive particles on the workpiece [25]. Miller proposed another equation for the material removal rate taking into consideration the amount of plastic deformation undergone by the workpiece per blow and other parameters [26]. Cook estimated the penetration rate as a function of common USM parameters such as the vibration amplitude, frequency, abrasive particle sizes and the workpiece hardness [27]. Since these were the parameters of interest for HR-μUSM, Cook's model was used in this analytical study. In this model the machining rate (MR) in the vertical direction (in mm s^{-1}), or the penetration rate, can be expressed by [27]:

$$\mathrm{MR} = 5.9f\left(\frac{\sigma}{H}\right)A^{0.5}R^{0.5} \tag{1}$$

where H is the hardness of the workpiece material (in kgf mm^{-2}), R is the mean radius of the abrasive grains (in mm), σ is the static stress applied in the cutting zone (in kgf mm^{-2}), A is the amplitude of vibration (in mm), and f is the frequency of oscillation. Equation (1) does not apply to the tools used in USM because they are typically ductile. Figure 2 shows the dependence of machining rate on the abrasive particle sizes (10–100 nm) and the vibration amplitudes (0.1–1.0 μm) of the USM micro-tool tip based on equation (1). The hardness of fused silica was set to 8.8 GPa [7]. Frequency of oscillation was set to 20 kHz. As seen in the graph, a decrease in R and A leads to a significant decrease in MR. The analysis suggests that a machining rate of approximately 5–15 μm min^{-1} (80–250 nm s^{-1}) is theoretically possible using ≈10 nm abrasive particle sizes and <1 μm tool vibration amplitude. This sets the targets for the vibration amplitude and abrasive particle sizes required for HR-μUSM.

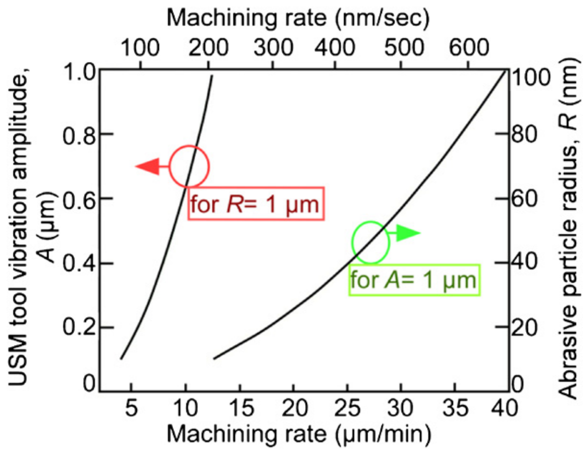

Figure 2. Dependence of machining rate on abrasive particle size and tool vibration amplitude based on equation (1). The use of ≈10 nm abrasive particle sizes and <1 μm tool vibration amplitude theoretically allows machining rates of approximately 5–15 μm min^{-1} (80–250 nm s^{-1}).

2.2. Instrument and material choices

For this work, the AP-1000™ stationary, benchtop USM machine (Sonic-Mill®, Albuquerque, NM, USA) was used as the ultrasound generator. Two horizontal stages and one vertical stage (Horizontal: M-505.2DG, Vertical: M-501.1DG, from Physik Instrumente®, Auburn, MA, USA) were integrated to form this *XYZ* stage system and resolves the workpiece movement to within 50 nm. A process control software was written in Visual Basic 2012. The software allows the manual movement of the *XYZ* stages for workpiece loading and micro-tool alignment and the control of the starting distance before performing HR-μUSM. A monoscope, capable of 200 × magnification, was used for alignment to the target location of the workpiece. A calibration procedure was implemented to measure the relative position between the monoscope and the micro-tool tip. This allowed accurate alignment of the micro-tool and workpiece with repeatable misalignment errors <1 μm. Figure 3 shows the customized system for HR-μUSM. The amplitude of vibration of the micro-tool depends on the ultrasound generator and the horn assembly that couples the vibration to the tool. A conventional USM machine utilizes a coupler that maintains the amplitude (i.e., a 1:1 coupler) or increases it. Maximizing the vibration amplitude allows higher machining rates. For HR-μUSM, however, the vibration amplitude must be attenuated in the coupler. For this work, a commercially available coupler with 50% attenuation (i.e., 1:2) was used (L02-0082, titanium coupler, Sonic-Mill®, Albuquerque, NM, USA). Table 1 compares important parameters of a conventional μUSM system and the customized system for HR-μUSM. The smaller vibration amplitudes and high resolution automated stages provide a platform upon which HR-μUSM based trimming can be further explored.

The material used for the micro-tool should have high wear resistance, favorable elastic and fatigue strength properties, toughness, and hardness [28–31]. Commonly used tool materials include tungsten carbide, steel, and

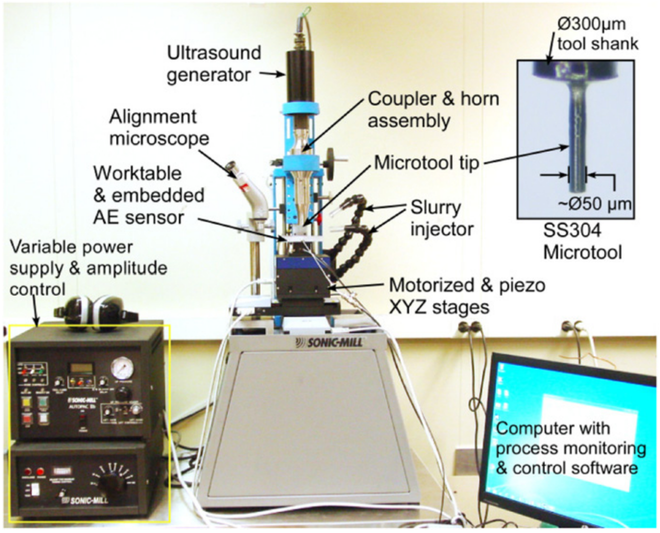

Figure 3. Photograph of the upgraded μUSM system showing various components.

Table 1. Comparison of conventional μUSM system parameters with that of the customized system for HR-μUSM.

	Conventional μUSM system	HR-μUSM system
Power supply	200–1000 W	200–1000 W
Coupler	1:1	1:2
Measured peak–peak vibration (μm)	15 μm @ $P = 20\%$	7 ± 1.5 @ $P = 20\%$
Vibration freq. (kHz)	20	20
Z-axis resolution	>1 μm	50 nm

Monel™ (which is an alloy of nickel, copper and iron). The dominant wear mechanism associated with tungsten carbide tools is diffusion of the tool material away from the cutting edge [32]. Stainless steel tools, however, have a lower tool wear ratio, i.e. the ratio of the tool height worn to the machined depth [9]. Stainless steel has a typical (Knoop) hardness of 138 and so is easier to machine than tungsten carbide (which has a typical Knoop hardness of 1870). A smaller tool diameter is favorable for precision, but presents challenges in tool fabrication and handling. A lower limit on the thickness of the micro-tool has been suggested of not less than five times the abrasive grit size [29, 30]. The micro-tool weight should be within the loading limits of the horn of the ultrasound generator. The screw attachment of a tool is known to reduce mechanical losses and increase machining efficiency [33–36], but this method is not generally amenable to attaching microfabricated tools.

The abrasive slurry used is another vital component in μUSM. As noted in section 1, the machining rate and surface roughness increase with the grain size of the abrasive used in the slurry. Conventional μUSM uses abrasive particle sizes ranging from 0.1–10 μm. In contrast, for this work, boron carbide and tungsten carbide abrasive powders with grain sizes as low as 100 nm are more appropriate. Commercially available diamond powders have grain sizes as low as 10 nm but can be quite expensive.

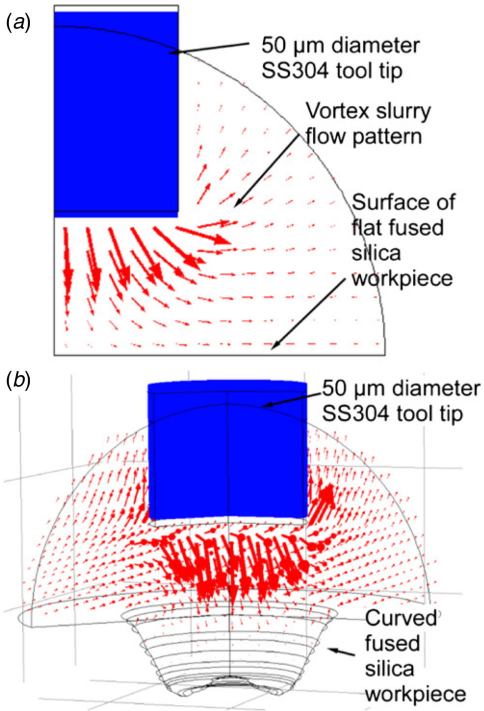

Figure 4. Results of FEA analysis showing slurry flow patterns during HR-μUSM of different workpiece profiles. (*a*) Vortex slurry flow pattern seen on a flat surface. The maximum slurry velocity observed on a flat fused silica substrate is 0.24 m s^{-1}. (*b*) Slurry flow pattern for a curved profile of 30 μm depth. Maximum fluid velocity observed on curved surface is negligible.

2.3. Finite element analysis of slurry flow patterns

Finite element analysis (FEA) can be used to assess the slurry flow patterns and velocities during HR-μUSM. The simulations use the acoustic-solid interaction module available in the acoustics model of COMSOL 4.3. A 2D axisymmetric geometry was developed. The geometry includes the end of a μUSM tool tip of 50 μm diameter. SS304 was used as the material for the micro-tool. The micro-tool was modeled at a fixed distance of 35 μm from the workpiece. The micro-tool was simulated to vibrate at a frequency of 20 kHz with a peak to peak amplitude of 7 μm. This reflects the vibration amplitude of the micro-tool tip measured using a laser displacement sensor. The slurry medium used was modeled as a liquid with properties that mimic those of typical water based slurries used in the experiments. Specifically, the density of the liquid was set to $\approx$1800 kg m^{-3}. Abrasive particles were not included in the simulations. The slurry flow pattern and the magnitude of the fluid velocity were measured on flat fused silica substrates.

The analysis revealed a vortex pattern of the slurry flow which explains the slight increase in machined feature diameter when compared to the tool size (figure 4(*a*)). This suggests a machined profile that is $\approx$1.3 $\times$ larger in diameter than the micro-tool. The magnitude of the fluid velocity had a maximum value of 0.24 m s^{-1} on the virgin fused silica substrate surface which was flat.

In order to study the change in slurry fluid velocity during machining, curved substrate profiles of depths varying from 10–30 μm were modeled. The curved profiles mimicked

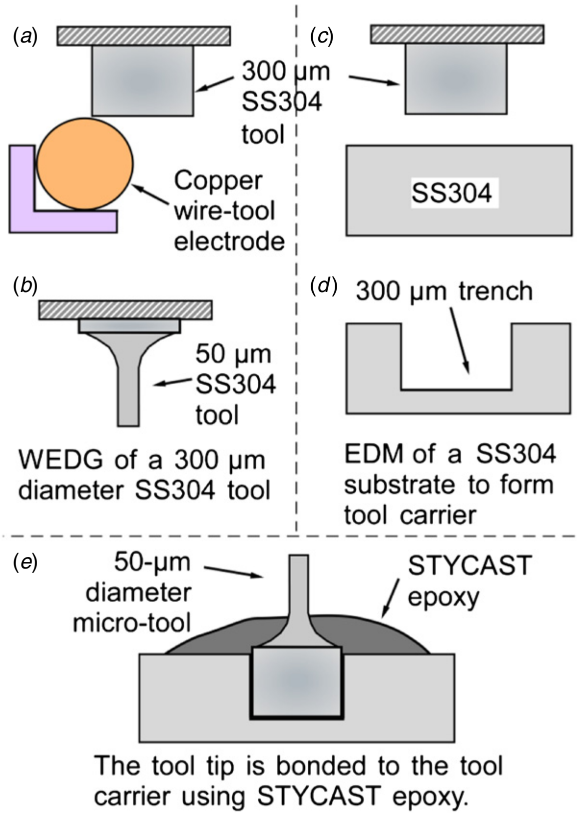

Figure 5. Conceptual diagram of serial mode fabrication of SS304 micro-tool. (*a*), (*b*) WEDG of a 300 μm diameter stainless steel (SS) tool in order to flatten the tip surface and then reduce the tool diameter. (*c*), (*d*) EDM of a SS substrate to form tool carrier to hold the tool perpendicularly. (*e*) The tool is inserted into the cavity of the tool carrier and bonded using STYCAST epoxy.

different stages of machined features as the μUSM machining was progressing. The slurry velocity magnitudes for each of these models were recorded. The slurry velocity observed at the surface of a 30 μm deep machined profile was negligible. Figures 4(*b*) shows the slurry flow pattern for a 30 μm deep machined profile.

3. Experimental evaluation

3.1. SS304 micro-tool preparation

The preparation of SS304 micro-tools of 50 μm diameter is described in figure 5. Wire electro-discharge grinding (WEDG) of 300 μm diameter SS304 wires is performed in order to flatten the tool tip as well as reduce the tip diameter to $\approx$50 μm (step 2(a)). Tip diameters as small as $\approx$5 μm can be fabricated by this method. The base of the tool is bonded into a cavity within a 1 mm thick planar SS304 housing, orienting the tool vertically. The cavity is formed by micro electro discharge machining (μEDM). This structure is bonded to a bolt that screws into the coupler-horn assembly of the USM machine using STYCAST epoxy. This process can be adapted to fabricate arrays of micro-tools for a batch mode trimming operation using the techniques described in [9]. For this effort, micro-tools of lengths ranging from 2–5 mm are used. The short micro-tools are used for HR-μUSM

Table 2. Machining rate as a function of fixed distance (FD) averaged over 1 min. 100 nm WC particles was used in the slurry.

Fixed distance (FD) (μm)	25	35	40
Simulated fluid velocity (m s^{-1})	0.35	0.19	0.09
Machining rate (nm s^{-1})	86.5	75.2	10.5

of flat fused silica substrates, whereas longer micro-tools are preferable for the machining of hard-to-reach surfaces of complex 3D workpieces.

3.2. Process characterization

The vibration amplitude of the micro-tool tip was measured using a laser displacement sensor (LK-G32 model, Keyence Corporation, IL, USA) with an accuracy of ≈1.5 μm. The sensor was focused on the surface of the vibrating head. The vibration amplitude had a peak-to-peak value of 7 ± 1.5 μm at 200 W input power. The lateral vibration of a 2 mm long tool was <1.5 μm. Machining characterization was performed on flat fused silica pieces of 90 μm thickness and 4 × 4 mm^2 area. Tungsten carbide (WC) powder (Inframat Advanced Materials, Manchester, CT, USA) of 100 nm particle size and diamond powder (Sigma-Aldrich Co., MO, USA) of 10 nm particle size were used in the machining evaluations. The slurry concentrations were WC:H_2O = 1:1 (by wt.) and diamond:H_2O = 1:5 (by wt.).

The experimental evaluation of the proximity of the micro-tool to the workpiece surface is presented in table 2. This evaluation was performed using 100 nm WC powder for an initial separation (denoted as FD in figure 1) varying from 25 to 40 μm in steps of 5 μm. The machining was performed for 1 min in each case. The machined depth of features was measured using an interferometer (LEXT™, Olympus Corporation, PA, USA). The machining rate provided in table 2 represents an average of three measurements clustered near the center of the machined feature. A maximum machining rate of 86.5 nm s^{-1} was observed when the FD was set to 25 μm. The increase in FD to 40 μm caused an 87% decrease in machining rate.

Machining was also performed for 35 μm FD while varying the machining time from 1 min to 10 min. This evaluation was performed for both 100 nm WC powder and 10 nm diamond powder. The maximum depths ranged from 20 to 60 μm for machining times ranging from 1 to 10 min (figure 6(*a*)). The machining rates saturated with time, ranging from >300 nm s^{-1} in the beginning to ≈100 nm s^{-1} at the end of the window (figure 6(*b*)).

Measurements show that the surface roughness of features machined with both the 100 nm WC and 10 nm diamond particles reduces as machining progresses (figures 7 and 8). The surface roughness was measured using an interferometer (LEXT™, Olympus Corporation, PA, USA). Surface finish was evaluated by measuring the average surface roughness (S_a) of different areas clustered near the center of the machined feature. Consistency was ensured by keeping the evaluation area for S_a constant across measurements. An average value was used to represent the surface roughness of a machined feature. The features machined for 3 min using 1 μm WC powder, which is traditionally used for μUSM, provided S_a of ≈245 nm (figure 8(*a*)). The features machined for 3 min, using WC powder of 100 nm particle size, provided S_a of ≈85 nm (figures 7 and 8(*b*)). The S_a for features machined with 10 nm diamond slurry powder was ≈30 nm (figures 7 and 8(*c*), (*d*)). The S_a of the virgin fused silica substrate was ≈5 nm. The average surface roughness achievable using conventional μUSM utilized in past work is typically 200–400 nm [8–11]. Table 3 provides the typical surface roughness

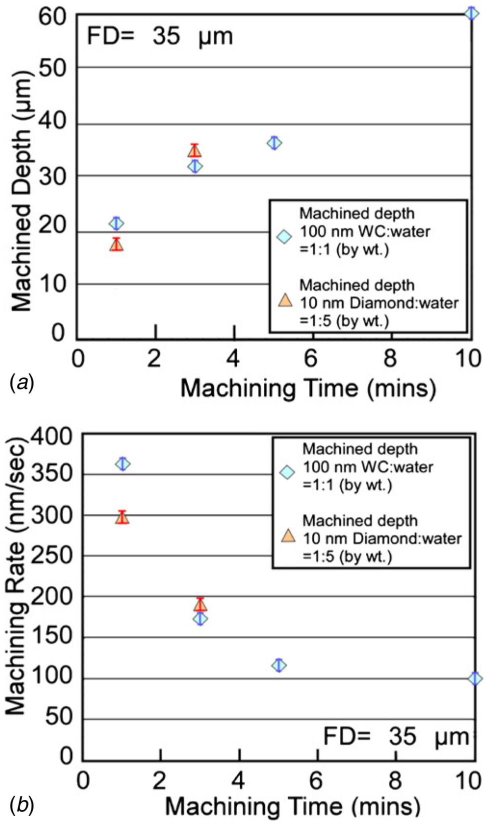

Figure 6. (*a*) Machining depth as a function of machining time. (*b*) Machining rate as a function of machining time. Machining rate averaged ≈100 nm s^{-1} at the end of the window.

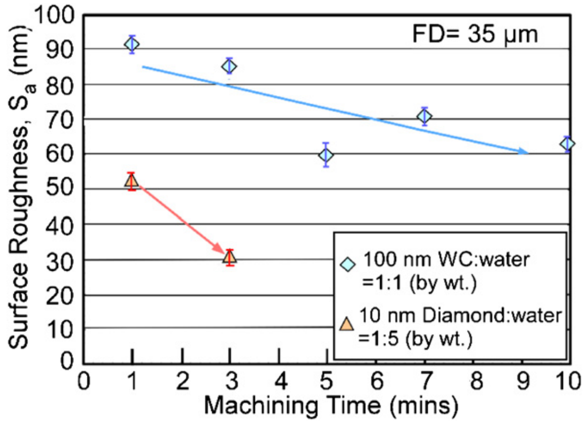

Figure 7. Average surface roughness, S_a, as a function of machining time. The minimum S_a observed was 30 nm; this was obtained with 10 nm diamond powder in 3 min.

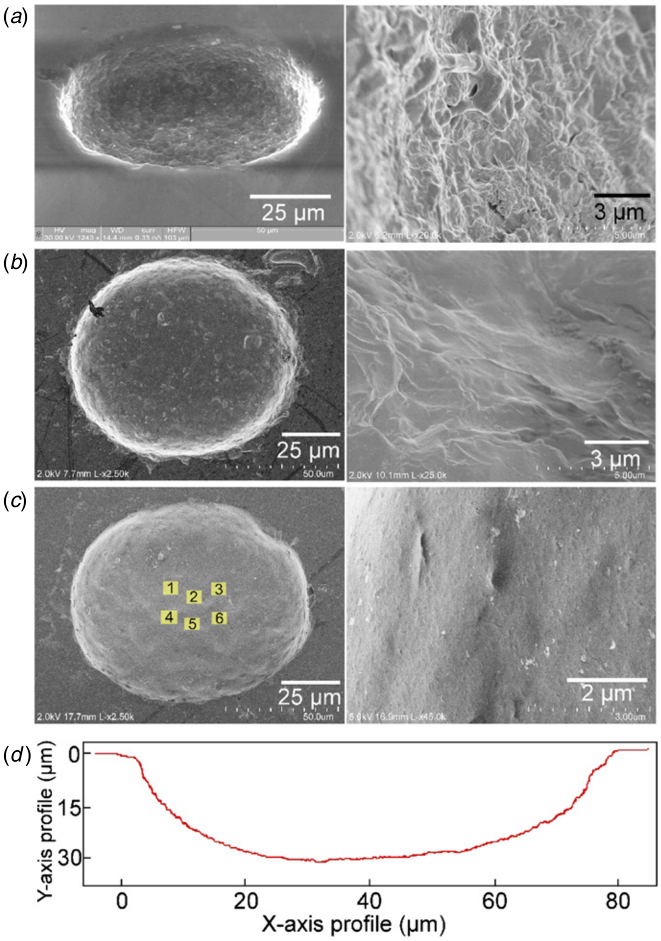

Figure 8. SEM images of machined features using: (*a*) tungsten carbide (1 μm, WC:H_2O = 1:1 by wt.). The machined feature diameter was 73 μm. The corresponding average surface roughness, S_a, was 245 nm. (*b*) Tungsten carbide (100 nm). The machined feature diameter was 69 μm. The corresponding S_a was 67 nm. (*c*) Diamond (10 nm) slurry. The machined feature diameter was 75 μm. The corresponding S_a was 30 nm. Each machining was performed for 2 min. (*d*) A typical profile of the machined feature using diamond (10 nm) slurry. Measured values of S_a at locations 1–6 denoted in (*c*) are provided in table 3.

Table 3. Average surface roughness (S_a) measured at six different areas of a feature machined with 10 nm diamond slurry powder (figure 8(*c*)).

Evaluation area	S_a (nm)
1	31
2	37
3	31
4	29
5	33
6	27
Average	≈30

parameters evaluated at six different areas in a feature machined using 10 nm diamond slurry powder (figure 8(*c*)). The S_a of features machined with 10 nm diamond particles is ≈7 × smaller than typical conventional μUSM.

Another parameter that can be used to assess surface quality is S_p, which represents the maximum height of peaks. In this work, for samples machined with 10 nm diamond particles, the S_p was ≈250 nm. The S_p can be greater than S_a due to factors such as minor imperfections of the tool and residual particles on the workpiece. A single defect can increase S_p even though the average roughness, as represented by S_a, may not be significantly affected by it. The average parameter S_a provides a surface roughness that better represents the majority of the area that has been machined and has been typically used to assess surface quality of machined features [8–11].

Table 4. Machining results for HR-μUSM.

Abrasive: avg. size (nm)	WC:100	Diamond:10
Min. cutting rate (nm s^{-1})	10	≈10
Roughness (S_a) (nm)	>60	30 or better

The average volume removed from virgin flat fused silica substrates in the first minute was $\approx 9.1 \times 10^{-6}$ mm^3. This corresponds to a mass removal of ≈20 ng min^{-1}. This estimate assumes that the machined profile can be approximated by a cone frustum. The wear length of the tool after machining of flat fused silica substrates was ≈1 μm. This corresponds to a tool wear ratio (i.e. ratio of the tool height worn to the machined depth) of <4%.

Table 4 summarizes the machining results. At 40 μm FD, the HR-μUSM process achieved cutting rates as low as 10 nm s^{-1}. The average surface roughness, S_a, achieved was ≈30 nm using 10 nm diamond particles in the slurry medium.

3.3. Application to trimming of 3D microstructures

The HR-μUSM process was applied to the trimming of hemispherical 3D microstructures made of fused silica. For this work, bird-bath (BB) shells (figure 9(*a*)), which are being investigated for use in rate integrating gyroscopes [7], were used. These structures have a diameter of 5 mm, and height of 1.55 mm, whereas the average thickness of the shell is only 70 μm. The BB shells are molded using a 3D μ-blow-torching process from fused silica. These shells have high mechanical quality factor, low stiffness and low damping anisotropy [7]. In general, trimming may be necessary at the surface of the rim, near the bottom of the shell, or at an intermediate location along the sidewall. Two different approaches are used to perform trimming in these locations and to accommodate the 3D nature of the workpiece, as illustrated in figure 10 and described below. In both cases, the BB shells are attached to a carrier substrate using standard 5 min epoxy (5 Min®, Devcon, MA, USA).

For machining the rim, the shells are potted in cyanoacrylate (Loctite®, Henkel Co., OH, USA) (figure 10(*a*)), before immersing in slurry. This arrangement provides mechanical support for the 70 μm thick shell walls, and also reduces the topographical variation, allowing the slurry flow to be similar to that for a flat substrate. This arrangement is also used when machining the sidewalls. For machining the bottom, the potting is not needed. Instead, slurry is filled into the shell, and a long tool (5–10 mm in length) is used to perform the trimming (figure 10(*b*)). The slurry

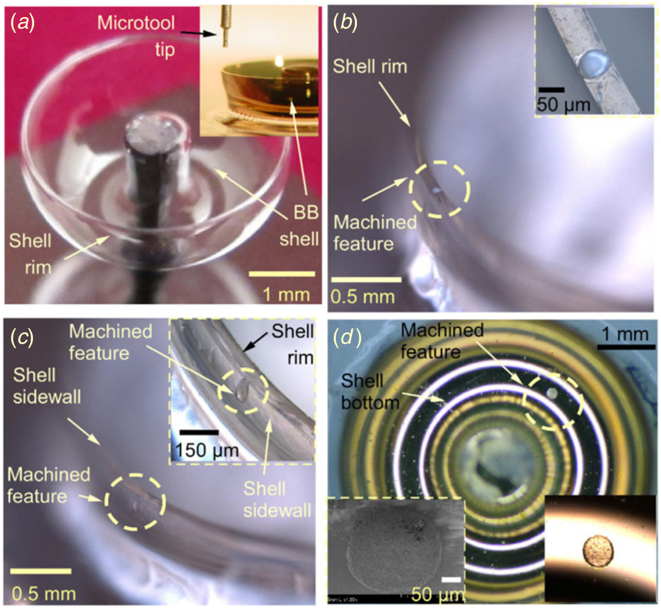

Figure 9. (*a*) A BB hemispherical shell of 5 mm diameter [7]. The inset shows a BB shell and the micro-tool after machining. (*b*)–(*d*) Results of trimming of BB shells using HR-μUSM. (*b*) Trimming of the top surface of the shell rim. Average machining rate measured was 102 nm s^{-1}. (*c*) Trimming of the outer sidewall of shell. Average machining rate measured was 84 nm s^{-1}. (*d*) Trimming of the bottom surface of the shell. Average machining rate measured was 60 nm s^{-1}.

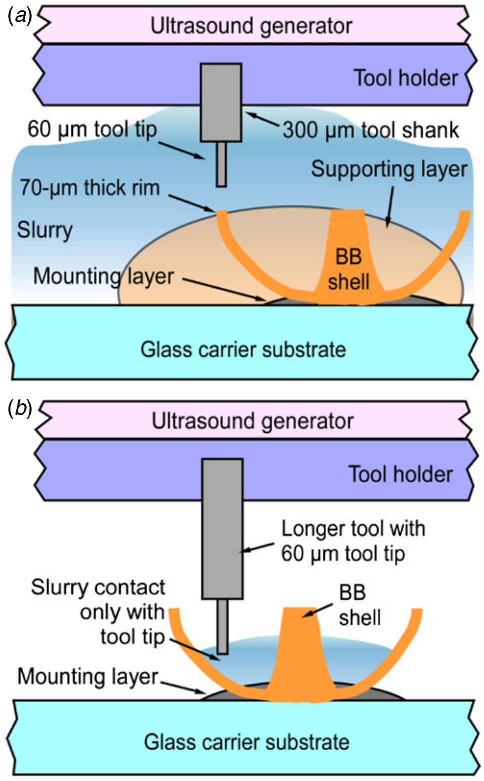

Figure 10. Modifications to tool/mounting configurations for trimming of BB shells. (*a*) Configuration A for shell rim and sidewall trimming: use of shorter tool lengths (2–5 mm) and adhesive layers around the shell for mechanical support. (*b*) Configuration B for shell bottom trimming: use of longer tools (5–10 mm) and slurry localized within the shell.

meniscus does not contact the tool holder, so the ultrasonic power is not directly transferred into the slurry. This reduces the propensity for damage to the fragile shell. The machined depth and surface roughness of features in the BB shells were measured using an interferometer (LEXT^{TM}, Olympus Corporation, PA, USA). The BB shells were coated with a ≈5 nm gold layer prior to measurement. This was done in order to facilitate laser interferometry and SEM imaging of the transparent and nonconductive fused silica shells, without significantly affecting the depth and roughness measurements.

Figure 9(*b*) shows a typical machined feature on the rim of the shell. Machining with 100 nm WC for 180 s provided an average depth of 18 μm, diameter of 60 μm, and roughness S_a of 120–150 nm. The tool diameter was 60 μm, and it was 2 mm long. Figure 9(*c*) shows a typical sidewall machined cavity. A machining time of 300 s provided a cavity with a typical maximum depth of 25 μm using 100 nm WC. The tool diameter and length were 120 μm and 5 mm, respectively. Figure 9(*d*) shows a typical machined cavity on the bottom surface of the shell. Tools of 120 μm diameter and 5 mm length were used. A machining time of 150 s, with 100 nm WC, provided features with 9 μm depth and 140 μm diameter. Compared to machining of the rim, the decrease in machining rate can be attributed to the smaller number of abrasive particles available for circulation in the cutting zone: some particles settle at the bottom of the shell and do not contribute to the machining. The average machining rate obtained during trimming at various locations of these shells was 80 nm s^{-1} for an FD of 35 μm. This is consistent with the characterization of the HR-μUSM process. The average volume removed from 70 μm thick molded fused silica shell in 3 min was ≈3.6 × 10^{-5} mm^3. This corresponds to a mass removal rate of ≈30 ng min^{-1}. The tool wear ratio was <4% for these samples.

4. Discussion and conclusion

The micro-tool fabrication sequence allows for flexibility of choice of micro-tool diameter and lengths. However, there are certain limitations to this technique. This is a serial process and involves manual mounting of a single micro-tool onto the USM tool head. This can be resolved by fabricating an array of micro-tools using the batch pattern transfer technique described in [9]. Another limitation is the micro-tool mounting error, i.e., the error in the orthogonality between the micro-tool and the workpiece. Although this does not have a major impact when machined features are shallow, such as those used for trimming, the tolerance is lower for deeper features. A monolithic approach to micro-tool fabrication will diminish this.

The typical machining rates of HR-μUSM demonstrated in this work averaged ≈100 nm s^{-1}, for 35 μm FD. The minimum machining rate was 10 nm s^{-1}, for 40 μm FD. This is an improvement in machining resolution over conventional machining technologies. The average mass of fused silica removed from a flat virgin sample in the first minute was

≈20 ng. An average surface roughness (S_a) of 30 nm was achieved by machining with 10 nm diamond abrasive particles in the slurry. This is ≈7 × smaller than typical conventional μUSM. The virgin fused silica workpiece surface has an average S_a of ≈5 nm and provides a quantitative comparison of smoothness achieved by HR-μUSM. It can be inferred by the experimental analysis that while the machining rate is influenced more by the separation between the tool and the workpiece, the surface roughness depends mainly on the abrasive particle size. A further decrease in vibration amplitude and abrasive particle sizes will facilitate lower machining rates and smoother profiles than that achieved in this work. The process was demonstrated for trimming of hemispherical 3D shells made of fused silica. Cavities were successfully formed on the thin shell rim with controlled depths and machining rates. A batch mode HR-μUSM process can be envisioned for batch mode post fabrication trimming of an array of 3D microstructures, improving the throughput. This will be pursued in future efforts.

Acknowledgments

The authors thank Professor K Najafi and Dr J Cho for providing the BB shells used in this work. This work was supported in part by DARPA MRIG award W31P4Q-11-1-0002.

References

[1] Hockin H, Xu K and Jahanmir S 1995 Microfracture and material removal in scratching of alumina *J. Mater. Sci.* **30** 2235–47

[2] Yan M F, Niwa K, O'Bryan H M and Young W S (ed) 1987 *Ceramic Substrates and Packages for Electronic Applications, Advances in Ceramics* vol 26 (Westerville, OH: American Ceramic Society) pp 525–41

[3] Palmer D W 1999 High-temperature electronics packaging *High Temperature Electronics* ed R Kirschman (New York: IEEE Press)

[4] Otsuka K 1993 *Multilayer Ceramic Substrate-Technology for VLSI Package/Multichip Module* (London: Elsevier)

[5] Tressler J F, Alkoy S and Newnham R E 1998 Piezoelectric sensors and sensor materials *J. Electroceram.* **2** 257–72

[6] Li T, Gianchandani R Y and Gianchandani Y B 2007 Micromachined bulk PZT tissue contrast sensor for fine needle aspiration biopsy *Lab on a Chip* **7** 179–85

[7] Cho J, Woo J, Yan J, Peterson R L and Najafi K 2014 Fused silica micro birdbath resonator gyroscope (μ-BRG) *J. Microelectromech. Syst.* **23** 66–77

[8] Sun X, Masuzawa T and Fujino M 1996 Micro ultrasonic machining and its applications in MEMS *Sensors Actuators* A **57** 159–64

[9] Li T and Gianchandani Y B 2006 A micromachining process for die-scale pattern transfer in ceramics and its application to bulk piezoelectric actuators *J. Microelectromech. Syst.* **15** 605–12

[10] Li T, Visvanathan K and Gianchandani Y B 2014 A batch mode micromachining process for spherical structures *J. Micromech. Microeng.* **24** 025002

[11] Yu Z, Hu X and Rajurkar K P 2006 Influence of debris accumulation on material removal and surface roughness in micro ultrasonic machining of silicon *Ann. CIRP* **55** 201–4

[12] Drozda T J and Wick C 1983 *Tool and Manufacturing Engineers Handbook: Machining* 4th edn vol 1 (Dearborn, MI: Society of Manufacturing Engineers)

[13] Moreland M A 1988 Versatile performance of ultrasonic machining *Am. Ceram. Soc.* **67** (6) 1045–7

[14] Perkins J 1972 An outline of power ultrasonics *Ultrasonics* **10** 288

[15] Farago F T 1980 *Abrasive Methods Engineering* vol 2 (New York: Industrial Press) pp 480–1

[16] Scab K H W 1990 Parametric studies of ultrasonic machining *Technical Paper* MR90-294 (Dearborn, MI: Society of Manufacturing Engineers) p 11

[17] Balamuth L 1964 Ultrasonic vibrations assist cutting tools *Metalwork. Prod.* **108** (24) 75–77

[18] Kremer D 1991 New developments on ultrasonic machining *Technical Paper* MR91-522 (Dearborn, MI: Society of Manufacturing Engineers) p 13

[19] Clifton D, Imai Y and McGeough J A 1993 Some ultrasonic effects on machining materials encountered in the offshore industries *Int. MATADOR Conf. (London)* pp 119–23

[20] Moreland M A 1984 Ultrasonic impact grinding: what it is: what it will do *Proc. Abrasive Engineering. Society Conf.: Abrasives and Hi-Technology* pp 111–7

[21] Kempe V 2011 *Inertial MEMS Principles and Practice* (Cambridge: Cambridge University Press)

[22] VanBeek J T M and Puers R 2012 A review of MEMS oscillators for frequency reference and timing applications *J. Micromech. Microeng.* **22** 013001

[23] Komaraiah M and Reddy P N 1993 A study on the influence of workpiece properties in ultrasonic machining *Int. J. Mach. Tools Manuf.* **33** 495–505

[24] Viswanath A, Li T and Gianchandani Y B 2014 High resolution micro ultrasonic machining (HR-μUSM) for post-fabrication trimming of fused silica 3D microstructures *MEMS'14: Int. Conf. on Micro Electro Mechanical Systems (San Francisco, CA, USA)* pp 494–7

[25] Shaw M C 1956 Ultrasonic grinding *Micro-Tech.* **10** (6) 257–65

[26] Miller G E 1957 Speed theory of ultrasonic machining *J. Appl. Phys.* **28** 149–56

[27] Cook N H 1966 *Manufacturing Analysis* (Reading, MA: Addison Wesley) pp 133–8

[28] McGeough J A 1988 *Advanced Methods of Machining* (London: Chapman and Hall) pp 170–98

[29] Kennedy D C and Grieve R J 1975 Ultrasonic machining—a review *Prod. Eng.* **54** 481–6

[30] Neppiras E A 1956 Report on ultrasonic machining *Metalwork. Prod.* **100** 1283–8

[31] Thoe T B, Aspinwall D K and Wise M L H 1995 The effect of operating parameters when ultrasonic contour machining *IMC'12: Irish Manufacturing Committee Conf. (Cork, Ireland)* pp 305–12

[32] Adithan M 1974 Tool wear studies in ultrasonic drilling *Wear* **29** 81–93

[33] Moore D 1985 Ultrasonic impact grinding *Proc. Non-traditional Machining Conf. (Cincinnati)* pp 137–9

[34] Shaw M C 1996 *Principles of Abrasive Processing* (Oxford: Clarendon)

[35] Prabhakar D and Haselkorn M 1992 An experimental investigation of material removal rates in rotary ultrasonic machining *Trans. NAMRI/SME* **20** 211–8

[36] Wojchiechowski M P 1972 Ultrasonic machining: past, present and future *Technical Paper* MR72-188 (Dearborn, MI: Society of Manufacturing Engineers) p 12